Numerical simulations of one-dimensional solitons

N. R. Pereira and R. N. Sudan

Laboratory of Plasma Studies, Cornell University, Ithaca, New York 14853

J. Denavit

Technological Institute, Northwestern University, Evanston, Illinois 60201
(Received 14 June 1976)

Numerical simulations of (i) the propagation and interactions of one-dimensional Langmuir solitons and (ii) their generation from random fluctuations by an external pump field are presented. The results of particle simulations are compared with computations based on Zakharov's fluid model. Those computations establish that Langmuir solitons are reasonably long lived entities in one dimension and are accurately described by Zakharov's equations, provided that resonant particle interactions are taken into account by the inclusion of a damping term. The power spectrum of the electron field fluctuations resulting from the generation of many solitons by an external pump field is compared with the theory of Kingsep, Rudakov, and Sudan.

I. INTRODUCTION

The concept of weak turbulence[1] has played a large role in the theory of Langmuir (plasma wave) turbulence excited by beam-plasma interaction. A warm electron beam propagating in a plasma excites Langmuir waves of frequency $\omega \approx \omega_e(1+\frac{3}{2}k^2\lambda_D^2)$ by resonant interaction; here, ω_e is the plasma frequency and λ_D is the Debye length. As the amplitude of this primary spectrum builds up nonlinear interaction between the waves becomes significant. This interaction is described in terms of three-wave and higher order processes. In a plasma where the electron and ion temperatures are equal, ion acoustic waves are disallowed so that the spectrum only consists of Langmuir waves. Since their dispersion relation is of the nondecay type, the total number of Langmuir waves is preserved and higher order processes can only transfer wave energy to longer wavelengths. Thus, the conclusion from weak turbulence appears to be that wave energy generated at $k \approx k_0 = \omega_e / v_0$ (v_0 is the beam velocity) passes to longer wavelengths. Since energy absorption at $k \to 0$ is negligible, this creates somewhat of a paradox unless other physical processes like finite physical boundaries, nonlinear conversion to photons which are then radiated, etc., are introduced.

On the other hand, several numerical computations of this problem[2-5] report significant departures from this conclusion of weak turbulence theory as the beam energy density is made a significant fraction of the plasma energy. The option of heating a cold or warm plasma by a powerful relativistic electron beam to thermonuclear temperatures presents a strong incentive to study this regime. Similar considerations appear in the analogous problem of plasma heating by a powerful coherent laser radiation.

If the spectrum frequency bandwidth $\Delta\omega$ is sufficiently small, then the assumption of weak turbulence (which requires $\Delta\omega$ to be greater than some critical value like γ, the growth rate of the waves) is no longer tenable. For resonant interaction $\Delta\omega/\omega \simeq k_k^2\lambda_D^2$ with $k \sim k_0 \sim \omega_e / v_0$ and $\gamma/\omega_e \sim n_b/n_0$, where n_b and n_0 are the beam and plasma densities, respectively. Now, $\Delta\omega \sim \gamma$ implies $n_b m v_b^2 \sim n_0 T_e$, where T_e is the electron temperature. Thus, if the beam energy approaches or exceeds the plasma thermal energy, we cannot expect to have weak turbulence. Alternatively, if the amplitude of the wave spectrum is very large we may violate the assumption of weak turbulence as follows: The time-averaged effect of a large amplitude high frequency electric field is equivalent to a force $-\nabla |E|^2/8\pi$ which creates an ion density perturbation $|\delta n/n_0| \approx -|E|^2/8\pi n_0 T_e$. This inhomogeneity in the plasma density creates a plasma frequency bandwidth $\delta\omega/\omega \approx \frac{1}{2}\delta n/n_0 \approx |E|^2/8\pi n_0 T_e$. When this self-induced bandwidth approaches or exceeds the natural bandwidth $k^2\lambda_D^2$, i.e., when $|E|^2/8\pi n T_e \gtrsim k^2\lambda_D^2$, we are again in conflict with weak turbulence.[6]

In situations where either $\Delta\omega$ is too small or $|E|^2$ too large in the manner discussed here, nonlinear processes called parametric instabilities with growth rate proportional to $(|E|^2/8\pi n T_e)^{1/2}$ dominate processes defined by weak turbulence whose growth rates are proportional to $|E|^2 8\pi n T_e$. For example, in a plasma with $T_e \gg T_i$ the three-wave "decay instability" of Oraevskii and Sagdeev,[7] in which a Langmuir wave decays into an acoustic wave and another Langmuir wave has a growth rate proportional to $(\omega_0\omega_s)^{1/2}(|E|^2 8\pi n T_e)^{1/2}$, where ω_0 and ω_s are the frequencies of the Langmuir and acoustic waves, respectively. This process is disallowed when $T_e \lesssim T_i$; but, in this case, if the pump wave has a frequency $\omega \approx \omega_e$, Nishikawa[8] has shown the existence of the so-called "oscillating two-stream" instability, in which ion fluctuations induced by the pump wave scatter the energy of electron oscillations to short wavelengths. This is really a four-wave process in which the scattered wavelength is approximately equal to the ion fluctuation wavelength $2\pi/k'$ and the scattered frequency ω' is approximately equal to ω, the pump frequency. The phase velocity of the scattered wave is much shorter than that of the pump wave since $k' \gg k$ and in consequence, its Landau damping is much larger. Thus, this parametric instability transfers energy from long wavelengths to shorter wavelength where it gets absorbed, a conclusion opposite to that obtained from weak turbulence theory.

The one-dimensional numerical simulations of Kainer *et al.*[2] were the first to see this effect of energy trans-

fer to shorter wavelengths, and this conclusion was reinforced more spectacularly by the laser-pump simulations of deGroot and Katz[4] and the relativistic electron beam-plasma interaction simulations of Thode and Sudan.[5] In the latter two particle simulations the one-dimensional power spectrum developed at long times as k^{-2}, between $10^{-2} < k\lambda_D < 1.0$. An explanation for this particular dependence was put forward by Kingsep *et al.*[9] in terms of the following picture. The beam driven primary spectrum pumps energy via the parametric instability to shorter wavelengths. However, this spectrum in k space can also be viewed in physical space as a random collection of solitons with a certain distribution. A soliton is a localized, stationary, large amplitude plasma wave in which the dispersive effect on the wave packet $k^2\lambda_D^2$ is balanced by the self-trapping effect of the induced ion density depletion $\delta n/n_0 \approx -|E|^2/8\pi n_0 T_e$. The equilibrium distribution of these solitons obtained from the principle of detailed balance furnishes the k^{-2} spectrum.

The objectives of the computations of the present paper are: (i) to establish that the soliton is a reasonably stable entity in one dimension for the purpose of the theory of Kingsep *et al.*[9]; (ii) to make a careful comparison of the excitation, propagation, and interaction of solitons on a particle simulation model and a fluid model based on Zakharov's equations,[10] and (iii) to compare spectra generated in the fluid model with the above-mentioned theory, and to reconcile differences between the two.

The plan of this paper is as follows. Section II gives a brief mathematical introduction leading to the numerical simulation methods discussed in Sec. III. Section IV discusses the numerical calculations of soliton propagation and collisions between solitons. We find that the results from the fluid code are in reasonable agreement with those from the particle simulation code provided the effect of electron Landau damping is suitably included in the fluid code.

In Sec. V it is shown that solitons can be generated from thermal noise fluctuations by an external pump electric field at $\omega = \omega_e$. For short systems of length L comparable to the wavelength λ of the most unstable mode of the parametric instability, the results obtained from particle and fluid simulations are compared. In both simulations the total electrostatic energy saturates at the same level and a soliton is observed. For long systems, $L \gg \lambda$, fluid simulations only were carried out. In this case many solitons are generated and the power spectrum of the resulting "soliton turbulence" is compared with the predictions of Kingsep *et al.*[9]

We note that Langmuir solitons, while stable in one dimension, are unstable in two or three dimensions to transverse perturbations.[11,12] A two-dimensional fluid model with Landau damping included has been used in detailed studies of this instability,[13] to be presented in a future paper.

II. DYNAMICAL EQUATIONS

To establish the notation and the equations used later in numerical computations, in this section we summarize the basic formulation and assumptions that lead to Zakharov's model for Langmuir soliton behavior.[10] Let δn_i denote the ion density perturbation and $\delta\tilde{n}_e$ denote the high-frequency component of the electron density perturbation. Setting the low frequency component of the electron density perturbation, δn_e, equal to the ion density fluctuation yields

$$n_i = n_0 + \delta n_i,$$

$$n_e = n_0 + \delta n_e + \delta\tilde{n}_e = n_i + \delta\tilde{n}_e,$$

where n_i, n_e, and n_0 denote, respectively, the ion density, the electron density, and the average ion (or electron) density. Neglecting the nonlinear electronic terms $\nabla\cdot(\delta\tilde{n}_e\delta\tilde{\mathbf{v}}_e)$ and $\delta\tilde{\mathbf{v}}_e\cdot\nabla\delta\tilde{\mathbf{v}}_e$, where $\delta\tilde{\mathbf{v}}_e$ is the high frequency electron velocity, the equation of conservation of electrons, the electron momentum equation, and Poisson's equation give

$$\nabla\cdot\left[\frac{\partial^2\tilde{\mathcal{E}}}{\partial t^2} + \omega_e^2\left(1+\frac{\delta n_i}{n_0}\right)(\tilde{\mathcal{E}}+\tilde{\mathcal{E}}_0 - 3\lambda_D^2\nabla\nabla\cdot\tilde{\mathcal{E}})\right] = 0. \tag{1}$$

Here, a spatially homogeneous external field $\tilde{\mathcal{E}}_0 = \bar{\mathbf{E}}_0\cos\omega_0 t$ of amplitude $\bar{\mathbf{E}}_0$ and frequency ω_0 has been introduced, $\tilde{\mathcal{E}}$ denotes the high-frequency internal field, $\omega_e = (4\pi e^2 n_0/m_e)^{1/2}$ is the electron plasma frequency, $\lambda_D = v_e/\omega_e$ is the Debye length, v_e is the electron thermal velocity, and $-e$ and m_e are, respectively, the electron charge and mass. Now, writing $\tilde{\mathcal{E}} = \mathrm{Re}[\mathbf{E}(\mathbf{x},t)\times\exp(-i\omega_e t)]$, where the amplitude $\mathbf{E}(\mathbf{x},t)$ is slowly varying at the ion time scale, and neglecting the nonlinear dispersion term $\delta n_i\nabla(\nabla\cdot\mathbf{E})$, yields

$$\nabla\cdot\left[i\frac{\partial\mathbf{E}}{\partial t} + \frac{3}{2}\omega_e\lambda_D^2\nabla(\nabla\cdot\mathbf{E})\right] = \frac{1}{2}\omega_e\nabla\left(\frac{\delta n_i}{n_0}\mathbf{E}\right) + \frac{1}{2}\omega_e\mathbf{E}_0\cdot\nabla\left(\frac{\delta n_i}{n_i}\right)\exp(-i\Omega_0 t), \tag{2}$$

where $\Omega_0 = \omega_0 - \omega_e$.

From the linearized equations for the ion fluid we obtain

$$\frac{\partial^2\delta n_i}{\partial t^2} + \frac{1}{m_i}\nabla\cdot(en_0\tilde{\mathcal{E}} + \mathbf{F}_i - 3T_i\nabla\delta n_i) = 0, \tag{3}$$

where $\tilde{\mathcal{E}}$ is the low frequency component of the electric field, $\mathbf{F}_i = -(m_e/m_i)\nabla\langle|\tilde{\mathcal{E}}+\tilde{\mathcal{E}}_0|^2\rangle/8\pi$ is the ponderomotive force on the ions from the high frequency components of the electric field,[14] T_i is the ion temperature, and m_i is the ion mass. The low frequency component of the electric field is obtained by the force balance on the electron fluid,

$$-en_0\tilde{\mathcal{E}} + \mathbf{F}_e - T_e\nabla\delta n_e = 0, \tag{4}$$

where $\mathbf{F}_e = -\nabla\langle|\tilde{\mathcal{E}}+\tilde{\mathcal{E}}_0|^2\rangle/8\pi$ is the averaged pondermotive force on the electrons and T_e is the electron temperature. Substituting $\tilde{\mathcal{E}}$ from Eq. (4) into Eq. (3), setting $\delta n_e = \delta n_i$ and neglecting $\mathbf{F}_i \ll \mathbf{F}_e$ gives

$$\partial^2\delta n_i/\partial t^2 - c_s^2\nabla^2\delta n_i = (16\pi m_i)^{-1}\nabla^2\{|\mathbf{E}|^2 + \bar{\mathbf{E}}_0\cdot[\mathbf{E}\exp(i\Omega_0 t) + \mathrm{c.c.}]\}, \tag{5}$$

where $c_s = [(\gamma T_i + T_e)/m_i]^{1/2}$ is the ion acoustic speed and $\gamma = 3$.

Zahharov's model for Langmuir turbulence is defined

TABLE I. Units used in dimensionless formulation of Zakharov's model.

time	$\frac{3}{2}(m_i/m_e)\omega_e^{-1}$
space	$\frac{3}{2}(m_i/m_e)^{1/2}\lambda_D$
velocity	$c_S=(m_e/m_i)^{1/2}v_e$
electric field	$[(64\pi/3)n_0m_ec_S^2]^{1/2}$
ion density	$\frac{4}{3}(m_e/m_i)n_0$
energy density	$\frac{4}{3}n_0m_ec_S^2$

by Eqs. (2) and (5), which now include an external field oscillating near the plasma frequency. These equations may be written in dimensionless form as

$$\nabla\cdot\left\{i\frac{\partial\mathbf{E}}{\partial t}+\nabla\nabla\cdot\mathbf{E}\right\}=\nabla\cdot[N\mathbf{E}+N\bar{\mathbf{E}}_0\exp(-i\Omega_0t)], \tag{6}$$

$$\frac{\partial^2N}{\partial t^2}-\nabla^2N=\nabla^2\{|\mathbf{E}|^2+\bar{\mathbf{E}}_0\cdot[\mathbf{E}\exp(i\Omega_0t)+\text{c.c}]\}, \tag{7}$$

where N denotes the ion density perturbation, and the units are defined in Table I.

One-dimensional Langmuir solitons are traveling solutions of Eqs. (6) and (7) obtained by setting $\bar{\mathbf{E}}_0=0$.[15] Assuming an ion density perturbation of the form $N=N(x-v_gt)$, propagating at a group velocity v_g, yields $|E|^2=N(v_g^2-1)$ from which

$$E(x,t)=[2k_0^2(1-v_g^2)]^{1/2}\{\cosh[k_0(x-v_gt)]\}^{-1}\times\exp[i(k_1x-\Omega t)] \tag{8}$$

and

$$N(x,t)=-2k_0^2\{\cosh[k_0(x-v_gt)]\}^{-2}, \tag{9}$$

where $v_g=2k_1$ and $\Omega=k_1^2-k_0^2$. A soliton is completely defined by the parameters k_0 and k_1, with $k_1<\frac{1}{2}$.

The formation of a soliton depends on a competition between dispersion and nonlinear terms in Eq. (6). These terms must therefore be approximately equal, requiring that the electrostatic energy W_e satisfy the condition $(k\lambda_D)^2\sim W_e/n_0T_e$ for values of k corresponding to the dominant waves of the spectrum. The nonlinear electronic terms which have been neglected in the derivation of Eq. (2) become significant for times larger than $\tau_{ne}=[\omega_e(k\lambda_D)^2\,W_e/n_0T_e]^{-1}$. Since soliton propagation occurs over times of order $(m_i/m_e)\omega_e^{-1}$, soliton behavior may be expected in the regime defined by the conditions

$$W_e/n_0T_e\sim(k\lambda_D)^2<(m_e/m_i)^{1/2}. \tag{10}$$

The effects of wave-particle interactions on the evolution of solitons can be included in Zakharov's model by introducing damping terms corresponding to Landau damping of the high and low frequency waves on the electron.[13,16] These terms are conveniently introduced into the spectral representation of Eqs. (6) and (7) which form the basis for the numerical solution. Reducing Eqs. (6) and (7) to one dimension, taking a Fourier transform with respect to the space variable, and introducing damping terms corresponding to each mode yields

$$i(dE_k/dt)-(k^2-i\gamma_k)E_k=(NE)_k+N_k\bar{E}_0\exp(-i\Omega_0t), \tag{11}$$

$$d^2N_k/dt^2+2\Gamma_k(dN_k/dt)+k^2N_k=-k^2(|E|^2)_k-\bar{E}_0k^2[E_k\exp(i\Omega_0t)+E_{-k}^*\exp(-i\Omega_0t)]. \tag{12}$$

Here, E_k, N_k, $(NE)_k$, and $(|E|^2)_k$ denote the Fourier transforms of the corresponding functions of the space variable. The constants γ_k and Γ_k account, respectively, for Landau damping of the high and low frequency waves. In dimensionless units these constants are given by

$$\gamma_k=\frac{3}{2}\frac{m_i}{m_e}\left(\frac{\pi}{8}\right)^{1/2}(k\lambda_D)^{-3}\exp[-\tfrac{1}{2}(k\lambda_D)^{-2}-\tfrac{3}{2}] \tag{13}$$

$$\Gamma_k=\frac{3}{2}\frac{m_i}{m_e}\left(\frac{\pi}{8}\right)^{1/2}\frac{1}{k\lambda_D}\left(\frac{\Omega_k}{\tilde{\omega}_p}\right)^2, \tag{14}$$

where Ω_k is the frequency of the ion motion for mode k.

Introducing the integral

$$I_1=\int_{-\infty}^{+\infty}[|E+\bar{E}_0\exp(-i\Omega_0t)|^2-\bar{E}_0^2]\,dx=2\pi\int_{-\infty}^{+\infty}E_kE_k^*\,dk+2\pi\bar{E}_0\mathrm{Re}[E_{k=0}\exp(i\Omega_0t)], \tag{15}$$

Eqs. (11) and (12) give

$$\frac{dI_1}{dt}=-2\pi\int_{-\infty}^{+\infty}\gamma_kE_kE_k^*\,dk+2\pi\Omega_0\bar{E}_0\mathrm{Im}[E_{k=0}\exp(i\Omega_0t)]. \tag{16}$$

If $\bar{E}_0=0$ and $\gamma_k=0$, the integral I_1 reduces to Zakharov's first invariant. In the case of an external driving field oscillating at the plasma frequency ($\Omega_0=0$), the integral I_1 decays ($\gamma_k>0$) or remains constant ($\gamma_k=0$). Since the internal field energy cannot grow indefinitely while I_1 remains bounded, it follows that the oscillating two-stream instability resulting from such a driving field ($\Omega_0=0$) necessarily saturates when the internal field E becomes approximately equal to the external field $\bar{E}_0$, this saturation occurring even in the absence of damping.[17] The situation discussed here corresponds to a plasma dielectric in a capacitor driven by a current generator. The alternative condition, where the plasma is driven by a voltage generator, would demand that the amplitude of the net electric field $E_{k=0}+\bar{E}_0$ remain constant.

Since the derivation of Eq. (7) is based on linearized equations for the ion fluid and assumes charge neutrality, this equation does not include any nonlinear or dispersion terms. In the regime defined by (10), these terms are not significant, except for solitons with group velocities near the ion acoustic speed. When $1-v_g^2=|E^2|/N\to m_e/m_i$, then we have to include additional terms arising from the dispersion and nonlinearity of the ion motion. In this limit we obtain the Korteweg-deVries equation,[16] modified by the ponderomotive force term $-2\partial|E|^2/\partial x$, and transferring it to the laboratory frame we recover the equation derived by Makhankov,[18]

$$\frac{\partial^2N}{\partial t^2}-\frac{\partial^2N}{\partial x^2}-\frac{4}{3}\frac{m_e}{m_i}\left(\frac{\partial^4N}{\partial x^4}+\frac{1}{3}\frac{\partial^2N^2}{\partial x^2}\right)=\frac{\partial^2}{\partial x^2}|E|^2. \tag{17}$$

Solitons have been observed to be unstable in two dimensions. We note that although they are stable in one dimension, solitons cannot propagate adiabatically in a

one-dimensional medium in which the Debye length or the density are a function of position. This follows from the fact that the relations $\int |E|^2 dx = \text{const}$, $\int N dx = \text{const}$, and $|E|^2 = N(v_g^2 - 1)$ cannot be satisfied simultaneously when v_g changes as a result of inhomogeneity. Indeed, a solition propagating in an inhomogeneous medium will limit ion fluctuations to keep these quantities consistent with each other.[19]

III. SIMULATION METHODS

The results of computer simulations of soliton behavior, presented in Secs. IV and V, were obtained by particle simulations and by fluid simulations based on Zakharov's equations, extended to include damping terms and an external driving field. In both methods the computations were one-dimensional with spatial variation in the x direction, and either reflecting or periodic boundary conditions were used.

The particle simulations include two species representing electrons and ions with a mass ratio $m_i/m_e = 100$. The algorithm is based on the method of periodic smoothing in phase space.[20] In this method the x-v phase plane for each species, is covered with a rectangular grid and weighted simulation particles initially located at each grid point are advanced according to their self and externally applied fields for 5 to 20 time steps. The distribution functions are then reconstructed by distributing the weight of each simulation particle locally among neighboring grid points. New weighted particles representing the updated distribution functions are then set up and advanced, after which the procedure is repeated. The repeated reconstructions are effective to smooth local fluctuations in the distribution functions and thus eliminate the noise due to individual particle interactions. The absence of noise in the present method has been verified in very low amplitude simulations,[21] and is an important consideration in the present simulations, because of the relatively low amplitude of the perturbations involved ($W_e/n_0 T_e \sim 1\%$).

The fluid simulations are numerical solutions of the Fourier transformed equations (11) and (12). A system of length L is considered with discrete wavenumbers $k = 2\pi m/L$, where m is an integer. The linear terms in the left members of these equations are integrated exactly and increments due to the right members are applied using an implicit method with iterations. Modes corresponding to $-m_{\max} \leq m \leq m_{\max}$ are retained in the computations. The convolution sums required in the nonlinear terms are computed by transforming back to x space after the addition of zero modes to eliminate the periodicity in k space. This method is similar but not identical to the split-time-step Fourier method.[22] All computations are carried out in k space and representation in x space is used only in evaluating convolutions or for diagnostic purposes.

IV. PROPAGATION AND INTERACTIONS OF SOLITONS

In this section we present particle simulations of the propagation and interactions of solitons of sufficiently low amplitude to allow comparison with theory and with computations based on the fluid equations, including Landau damping, discussed in Sec II.

In the particle simulations, a soliton is initialized by setting up Maxwellian distribution functions of the form

$$f_s(x, v, t=0) = (n_s/\sqrt{2\pi v_s^2}) \exp[-(v - V_s)^2/2v_s^2],$$

for the ions ($s = i$) and for the electrons ($s = e$). The ion and electron density perturbations corresponding to a soliton are given by $\delta n_i = \delta n_0 + \frac{3}{4}(m_e/m_i) n_0 N(x, t=0)$ and $\delta n_e = \delta n_i - (4/3\sqrt{3})(m_e/m_i) n_0 \partial E/\partial x|_{t=0}$, where $N(x, t=0)$ and $E(x, t=0)$ are given by Eqs. (8) and (9) and the constant δn_0 is chosen to satisfy the condition $\int \delta n_i \, dx = 0$. In addition, we need initialization of the drift and thermal velocities. The low-frequency ion drift velocity V_i must satisfy the equation of continuity, from which $V_i = v_g \delta n_i / n_i$. The electron drift velocity is obtained from the conditon $\partial \tilde{\mathcal{E}}/\partial t = -4\pi e(n_i V_i - n_e V_e)$, from which $V_e = (\partial \tilde{\mathcal{E}}/\partial t)/4\pi e n_e + (n_i/n_e) V_i$, where $\tilde{\mathcal{E}} = 2\mathrm{Re}[E \exp(-i\omega_e t)]$. In addition to its low-frequency component V_i, the ion drift velocity also includes a high-frequency component $\tilde{V}_i = (m_e/m_i) V_e$. For the mass ratio $m_i/m_e = 100$ used in the present simulations, $|\tilde{V}_i/V_i| \sim (m_e/m_i)^{1/2} = 0.1$, and $\tilde{V}_i$ must therefore be included as a correction in the initialization of the ion drift velocity. Finally, the thermal velocities are specified by the one-dimensional adiabatic condition, $v_e = (n_e/n_0) v_{e0}$, $v_i = (n_i/n_0) v_{i0}$, where v_{e0} and v_{i0} are ambient values.

A uniform grid with mesh size $\Delta x = \lambda_D$ in space, and extending to $\pm 4.6\, v_{s0}$ with 61 grid points in velocity was used. The internal electric field was computed at time intervals $\Delta t = 0.2\, \omega_e^{-1}$ and the distribution functions were reconstructed every 10 time steps.

In the fluid computations, a soliton is initialized by simply setting up values of $E(x, t=0)$, $N(x, t=0)$, and $M(x, t=0) = \partial N/\partial t|_{t=0}$ obtained from Eqs. (8) and (9).

A. Soliton propagation

The evolution of the ion density fluctuation corresponding to the particle and fluid models, for a soliton with parameters $k_0 = 1$ and $v_g = 0.6$, are compared in Fig. 1. Parameters are given in the dimensionless units of Table I, except when stated otherwise. The length of the system, $L = 8.55$ was chosen to allow propagation of the soliton over a sufficient time, $t_{\max} = 2.13$, without significant interaction with the reflecting boundaries. These parameters correspond to $k_0 \lambda_D = 1/15$, $v_g = 0.6\, c_s$, $L = 128\, \lambda_D$, and $\omega_e t_{\max} = 320$.

The ion density perturbation from the particle simulation, shown by the solid line, propagates to the right and follows, approximately, the theoretical soliton behavior given by Eq. (9). However, the depth of the ion depression decreases as the soliton propagates and a tail appears in its trailing end. The position of the center of mass of the soliton as a function of time is shown in Fig. 2(a). To eliminate the effect of the tail, the center of mass is computed by considering only the central portion of the soliton, defined by $x_m - 2\Delta x_1 < x < x_m + 2\Delta x_2$, where x_m corresponds to the minimum of the ion density and Δx_1 and Δx_2 are the distances from the minimum where $\delta n_i = 0.5\, (\delta n_i)_{\min}$. We observe that the velocity of the center of mass follows closely the theo-

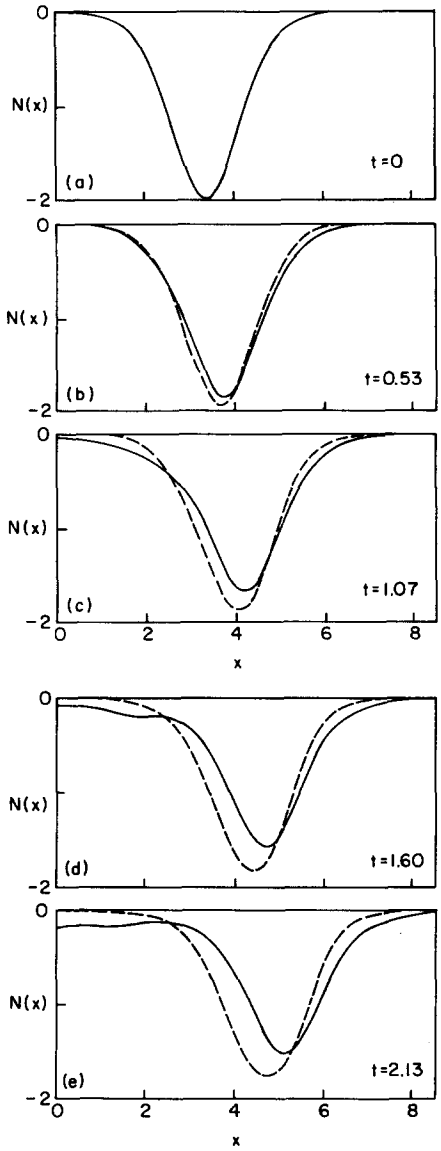

FIG. 1. The evolution of the ion density perturbation $N(x,t)$, calculated from particle simulation (solid line) and fluid code (broken line) as a function of x for different times. Initial parameters are $k_0 = 1.0$, $v_g = 0.6$.

retical group velocity given by the solid line in Fig. 2(a).

The ion density perturbation from the fluid equations, shown as a broken line in Fig. 1, agrees qualitatively with the particle simulation results. However, we observe that, in this simulation, no significant tail appears on the trailing end of the soliton. This computation includes Landau damping of the high frequency wave by the electrons which is responsible for the decay of the ion perturbation. An additional computation showed that including Landau damping of the low-frequency wave by the electron does not yield significantly different results. The position of the center of mass of the soliton, computed by the same method as in the particle simulation, is shown in Fig. 2(a) and close agreement is observed between the two models.

The electrostatic energy of a soliton is given in dimensionless units by $W_e = \frac{1}{2}\int |\mathrm{Re}([E\exp(-i\omega_p t)]|^2\, dx$. Substituting $E(x,t)$ from Eq. (8) into this integral yields

$$W_e = 4k_0(1 - v_g^2)\left\{1 + \frac{\pi k_1/k_0}{\sinh(\pi k_1/k_0)} \cos\left[2\left(\frac{3}{2}\frac{m_i}{m_e} - k_0^2\right)t\right]\right\}.$$

Thus, W_e oscillates about the average value $\langle W_e\rangle = 4k_0(1 - v_g^2)$ at approximately twice the plasma frequency. The maxima, minima, and average of the total electrostatic energy of the system, W_t, from the particle simulation are given in Fig. 2(b). Note that the difference between W_t and W_e represents electrostatic energy not trapped in the soliton. The average electrostatic energy remains constant, but a significant decay of the oscillation amplitude is evident. In the fluid simulation, the electrostatic energy is not followed on the electronic time scale but the average electrostatic energy, given by $\langle W_t\rangle = \frac{1}{2}\int EE^*\, dx$, decays due to Landau damping of the high frequency wave as shown by crosses in Fig. 2(b). The absence of any decay in the average electrostatic energy in the particle model shows that resonant electrons do not actually cause Landau damping but only an energy transfer between modes. However, the agreement in the decay of the soliton amplitude between particle and fluid simulations suggests that this energy transfer has approximately the same effect as Landau damping in the fluid code. This effect is to disrupt the balance between nonlinearity and dispersion which is required for theoretical soliton behavior. This interpretation is confirmed by simulation results for larger amplitude solitons and for the soliton collisions which follow.

The ion density fluctuations corresponding to the par-

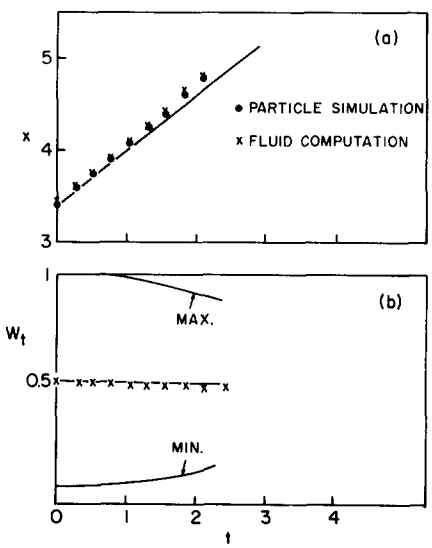

FIG. 2. (a) Position x of the center of mass of the solition as a function of time calculated from the particle simulation (circles) and from the fluid code (crosses). The predicted motion of the center of mass for the undamped soliton is given by the solid line. Initial parameters are $k_0 = 10$, $v_g = 0.6$. (b) The total electrostatic energy W_t as a function of time. For the particle simulation, W_t oscillates between a maximum and a minimum at about $2\omega_e$. The maximum, minimum, and average values are shown by respectively, upper, lower and middle lines. The crosses show the average electrostatic energy $\langle W_t\rangle$ from the fluid code.

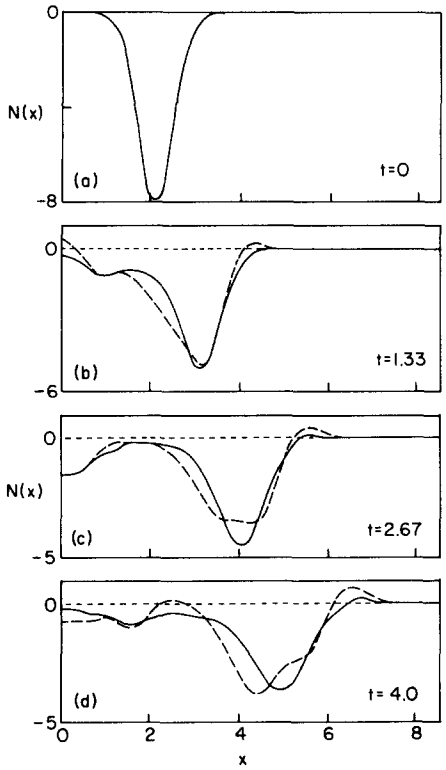

FIG. 3. The evolution of the ion density perturbation $N(x,t)$, calculated from particle simulation (solid line) and fluid code (broken line) as a function of x for different times. Initial parameters are $k_0=2.0$, $v_g=0.4$. The soliton decreases in amplitude, and ion acoustic waves appear at $t=1.33$.

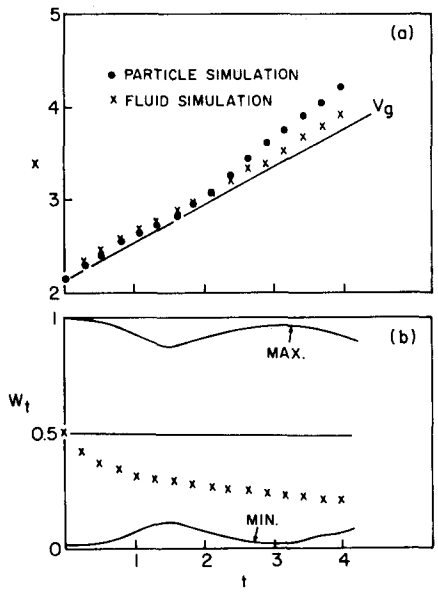

FIG. 4. (a) Position of the center of mass of the soliton as a function of time calculated from the particle simulation (circles) and from the fluid code (crosses). The predicted motion of the center of mass for the undamped soliton is given by the solid line. Initial parameters are $k_0=2.0$, $v_g=0.4$. (b) The total electrostatic energy W_t as a function of time. For the particle simulation, W_t oscillates between a maximum and a minimum at about 2 ω_e. The maximum, minimum, and average values are shown by, respectively, upper, lower, and middle lines. The crosses show the average electrostatic energy $\langle W_t \rangle$ from the fluid code.

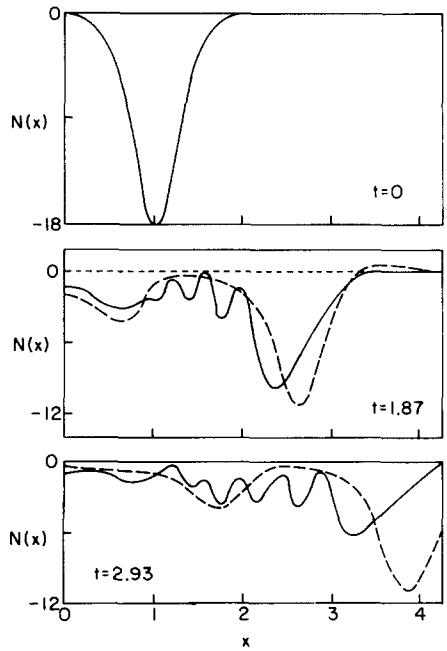

FIG. 5. The evolution of the ion density perturbation $N(x,t)$, calculated from particle simulation (solid line) and fluid code (broken line) as a function of x for different times. Initial parameters are $k=3.0$, $v_g=0.4$.

ticle and fluid models for a soliton of larger amplitude with $k_0=2$ and $v_g=0.4$, are compared in Fig. 3. A larger decay of the soliton occurs now than in the smaller amplitude case of Fig. 1, but the soliton amplitudes in the particle and fluid models are in good agreement. The detailed form of the soliton is distorted in both models and ion perturbations, which are not accompanied by any trapped electrostatic energy, appear in its trailing end. Since $k_0\lambda_D=0.13$ in the present case, strong wave-particle interactions are expected to occur for modes with wavenumbers $k \gtrsim 3k_0$. Indeed, we observe that the soliton decays most rapidly at the beginning of the simulation ($t<1.33$), corresponding to a truncation or rearrangement of its initial spectrum, while for later times ($t>1.33$) the ion density appears to settle to an approximate steady-state soliton of smaller amplitude ($k_0 \sim 1$) superimposed over ion acoustic waves.

The position of the center of mass, plotted as a function of time in Fig. 4(a), shows that the soliton propagates for both models with a group velocity slightly larger than the theoretical value. The maxima, minima, and average of the electrostatic energy W_t from the particle simulation, given in solid lines in Fig. 4(b), show that the average energy remains constant. The average electrostatic energy from the fluid code, given by the broken line, decays due to Landau damping as in the preceding simulation.

An additional larger amplitude case, with $k_0=3$, $v_g=0.4$ is given in Fig. 5. Here, there is a large distortion of the soliton, with significantly different behavior for the particle and fluid model, with the appearance of short wavelength oscillations which have no counterpart in the fluid model results.

It should be observed that nonlinear and dispersive effects which have been neglected in the equations may account for some differences between the preceding particle and fluid simulation results.[18] Although Eq. (17) is exact only in the limit $v_g \to 1$, it may be used to estimate the times τ_d and τ_{ni} after which ion dispersion and nonlinearities become significant. Equating the time derivative term to the dispersive term and to the nonlinear term in Eq. (17), for values of N corresponding to a Langmuir soliton, yields $\tau_d \simeq \tau_{ni} \simeq (m_i/m_e)^{1/2}/k_0^2$. For the simulation results of Fig. 1, $k_0 = 1$, these times ($\tau_d \simeq \tau_{ni} \simeq 10$) are clearly longer than the simulation time ($t_{max} = 2.17$). In the case of Fig. 3, the soliton decays rapidly to $k_0 \sim 1$ due to resonant particle effects. After this stage, $\tau_d \simeq \tau_{ni}$ are again longer than the simulation time and thus nonlinear and dispersive effects are unimportant. However, in the large amplitude case of Fig. 5, where $\tau_d \simeq \tau_{ni} \sim 1$, ion nonlinearities and dispersion are expected to have a significant effect which is included in the particle simulations but absent from the fluid model. This may explain the discrepancies evident in Fig. 5.

Finally, we observe that the electron trapping times $\tau_t \simeq 2\pi(eE_k k/m_e)^{-1/2}$(approximately 1 to 3 dimensionless units) in the preceding simulations, are typically shorter than the simulation times. However, electron trapping effects are not expected to occur because of the very short transit times (approximately 10^{-2} dimensionless units) of resonant particles across the solitons.

B. Collision between solitons

The interaction of two solitons has been studied by Abdulloev *et al.*[23] and by Degtyarev *et al.*[24] by numerical solutions of Zakharov's one-dimensional fluid equations excluding Landau damping,

$$i\frac{\partial E}{\partial t} + \frac{\partial^2 E}{\partial x^2} = NE, \tag{18}$$

$$\frac{\partial^2 N}{\partial t^2} - \frac{\partial^2 N}{\partial x^2} = \frac{\partial^2}{\partial x^2}|E|^2. \tag{19}$$

When the second order time derivative term in Eq. (19), which is due to ion inertia, is neglected, this equation yields $N = -|E|^2$ and the fluid model reduces to a single equation[10]

$$i\frac{\partial E}{\partial t} + \frac{\partial^2 E}{\partial x^2} + |E|^2 E = 0. \tag{20}$$

This equation, which has been treated extensively in the literature, satisfies an infinite number of invariants and is exactly integrable.[25] It admits soliton solutions of the form given by Eq. (8), with $v_g = 0$ in the numerator. Such solitons are stable and two colliding solitons always pass through each other, changing their velocity only during the interaction.

The system of equations (18) and (19) is not exactly integrable and is found to have properties very different from those of Eq. (20) when interactions between solitons are considered. In Ref. 23 the condition $I_1 > v_g(1 - v_g^2)$ is stated for the merging of two colliding solitons to form a single large-amplitude soliton. Numerical studies by Pereira[13] do not lead to such a simple condition and show that the initial phase difference between the solitons also plays an important role. In the case of coalescence, the collision between solitons is accompanied by emission of ion acoustic waves.

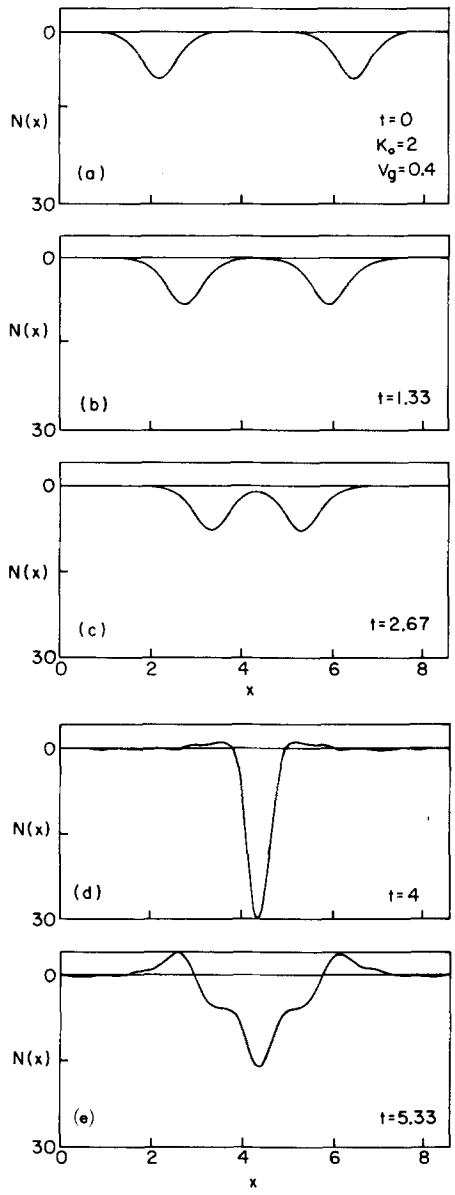

FIG. 6. The evolution of the ion density perturbation $N(x,t)$ for a collision between two identical solitons with opposite velocities as a function of x at different times in the undamped case. Initial parameters are $k_0 = 2.0$, $v_g = \pm 0.4$.

Here we consider the collision of two solitons of equal amplitudes with $k_0 = 2$, traveling with opposite group velocities $v_g = \pm 0.4$. The results of a particle simulation will be compared with fluid computations *including* Landau damping. However, to establish a basis of comparison, a computation based on Eqs. (18) and (19), i.e., excluding Landau damping is considered first. The results of this preliminary computation, given in Fig. 6, show that as they collide at $t = 4$, the solitons merge into a single large-amplitude soliton which is accompanied by the emission of an ion acoustic wave.

The results of the particle simulations and of the fluid

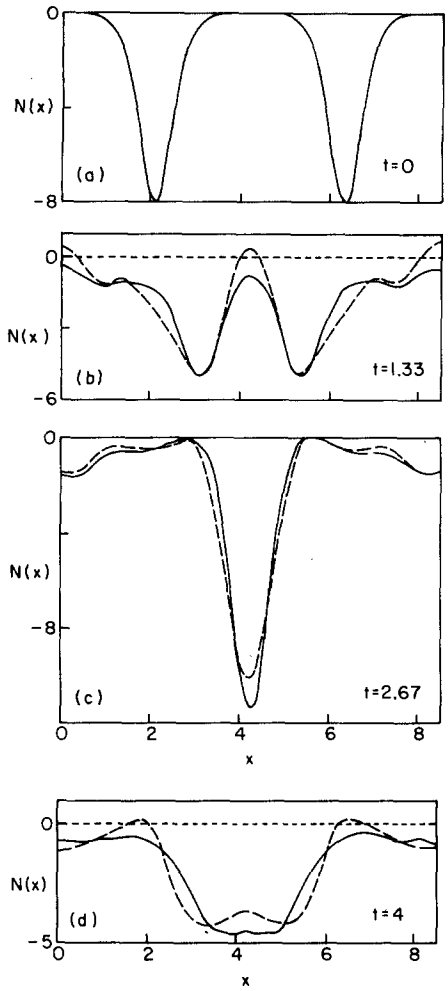

FIG. 7. The evolution of the ion density perturbation $N(x,t)$ for a collision between two identical solitons with opposite velocities as a function of x at different times, calculated from particle simulation (solid line) and fluid code with damping (broken line). Initial parameters are $k_0 = 2.0$, $v_g = \pm 0.4$.

computations including Landau damping, shown in Fig. 7, are very different from the preceding results. The approaching solitons propagate, as found earlier, at a group velocity somewhat larger than v_g and therefore collide at an earlier time, $t = 2.67$. As the collision occurs the resulting soliton now has a much smaller amplitude than in the solution without damping (note the scale difference between Figs. 6 and 7), and decays rapidly to form a single low-amplitude soliton at $t = 4$. There is a remarkably good agreement in Fig. 7 between the particle model and the fluid model including damping, when compared with the results of the fluid model excluding damping shown in Fig. 6.

In the absence of Landau damping or resonant particles, the soliton resulting from the collision in Fig. 6(d) has a parameter $k_0' \simeq 4k_0 = 8$, corresponding to $k_0'\lambda_D \simeq 0.5$, and its wave spectrum therefore extends into the region $k\lambda_D \sim 1$. In the presence of resonant particles this spectrum is therefore truncated in k space resulting in the broader and weaker soliton in x space found in the simulation results of Fig. 7 at $t = 4$.

V. SOLITON GENERATION

In this section we consider the generation of solitons from random initial fluctuations by an external pump field through the mechanism of the parametric instability. For a driving field frequency equal to the plasma frequency, $\Omega_0 = \omega_0 - \omega_e = 0$, in Sec. II we have seen that the integral $I_1 = \int (|E + E_0|^2 - E_0^2)\, dx$ satisfies the inequality $dI_1/dt \leq 0$ for $\gamma_k \leq 0$. Thus, for $\Omega_0 = 0$, the instability must saturate, even in absence of damping, when the energy of the internal field is approximately equal to the external field energy. After saturation, the electrostatic energy condenses into solitons each having an energy $\simeq \lambda_m E_0^2/8\pi$ spaced approximately λ_m apart, where λ_m is the wavelength of the most unstable mode. In particle simulations by Valeo and Kruer,[26] transient soliton type structures were generated by a powerful external field with normalized amplitude $\eta = E_0/(4\pi n_0 T_e)^{1/2} = 0.8$ and a frequency $\omega_0 = 0.9\,\omega_e$. These structures were found to have an amplitude corresponding to $k_0\lambda_D \sim 0.15$ which results in strong damping due to wave-particle interaction. The smaller values of the external field considered here, with η ranging from 0.125 to 0.25 allow us to generate stable solitons, having recognizable features.

A comparison between particle and fluid simulations of a single soliton is considered first. The generation of multiple solitons in a long system is then considered by fluid simulation alone.

A. Comparison of particle and fluid simulation of a single soliton generation

A particle simulation of the parametric instability was done with a system of length $L = 30\,\pi\lambda_D$, a mass ratio $m_i/m_e = 100$, and a driving field with a normalized amplitude $\eta = 0.16$, oscillating at the plasma frequency. All modes of the electron and ion density (up to $k_{max} = 2\pi \times 41/L$) were initially given small perturbations of equal amplitudes and random phases.

The same mass ratio, pump field, and system length were used in a fluid simulation. In this case, the computation is initialized by giving to electric field modes (up to $k_{max} = 2\pi \times 10/L$) equal initial amplitudes and random phases while the ion density is initially unperturbed.

The first mode $k = 2\pi/L$ is the most unstable and grows exponentially, in both simulations, until the energy of the internal field reaches a value approximately equal to the pump field energy. As the field energy approaches saturation it condenses into a single soliton.

The ion density profile when the soliton first appears is shown in Fig. 8(a). The solid line corresponds to the particle simulation at $t = 14$ while the broken line corresponds to the fluid computation, but at $t = 12.33$. The difference in time is caused by a slight difference in the early evolution of the instability. The amplitude of the soliton observed in the particle simulation reaches a maximum at $t = 15$, while the maximum in the fluid computation occurs at $t = 13.33$ and is significantly lower, see Fig. 8(b). After the maximum is reached, both $|E|^2$ and N decrease in the two computations and perturbations which leave the soliton region

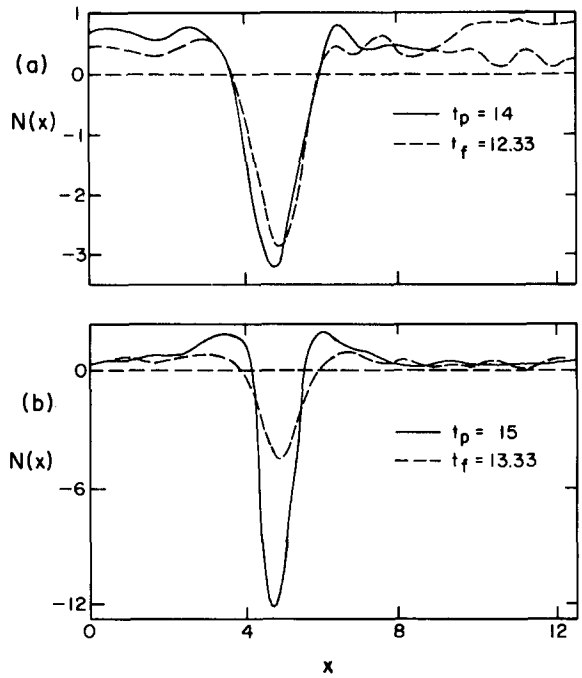

FIG. 8. Ion density profile $N(x,t)$ of a soliton generated by an external pump with $\eta = 0.16$. Solid lines correspond to the particle simulation (at times denoted by t_p) and broken lines correspond to the fluid computation (at times denoted by t_f).

are generated. In this later stage the maximum amplitudes of the solitons, in both computations, oscillate about somewhat different mean values.

We conclude that the two compuations agree quantitatively with one another for $t \lesssim 14$. At later times the qualitative features of the two computations are still in good agreement. Both computations exhibit saturation of the instability around $t = 15$ with formation of a single large soliton, and subsequent oscillations in the soliton amplitude, together with the appearance of perturbations in $|E|^2$ and N.

The late time spectrum of the electrostatic field in the particle simulation at $t = 17.8$ is given by the circles in Fig. 9, while the solid line shows the electrostatic field spectrum of a single Rudakov soliton, Eq. (8), with $k_0 = 2$.

For $k\lambda_D < 0.2$ (region I), the spectrum agrees with the k^{-2} dependence found in previous particle simulations.[4-6] However, for $0.2 < k\lambda_D < 0.7$ (region II) the spectrum falls off more rapidly, approximately as k^{-8}, while for even larger k, $k\lambda_D > 0.7$ (region III) the spectrum displays a tail approximately fitted by a k^{-4} power law. The single soliton spectrum agrees with the particle simulation spectrum out to $k\lambda_D = 0.7$ (regions I and II) but falls off more rapidly for larger values of k.

The low amplitude tail for $k\lambda_D > 0.7$ (region III) appears to be the result of errors due to the discrete representation of the electric field and of the distribution function. With mode energies which are six orders of magnitude lower than the large-amplitude modes near $k = 0$, this region of the spectrum is not expected to have a significant effect on the formation or the evolution of the soliton.

B. Multiple soliton generation

One-dimensional Langmuir turbulence has been described[9] as a random collection of solitons. To examine this concept, fluid simulations of the parametric instability were made with a long system $L = 2000\pi\lambda_D$, a mass ratio $m_i/m_e = 2000$, and driving fields with normalized amplitudes η ranging from 0.125 to 0.25 oscillating at the plasma frequency ($\Omega_0 = 0$). For the weaker pump field, $\eta = 0.125$, the maximum growth rate of the instability occurs for $k\lambda_D = 0.26$, corresponding to a wavelength $\lambda_m = L/26$, and therefore after saturation we expect to observe approximately 26 solitons.

The computation is initialized by giving to all electric field modes equal amplitudes $|E_k| = 10^{-5} E_0$ with random phases, where $k = 2\pi m/L$ and $|m| \leq m_{max} = 341$. Initially, the instability is observed to develop in agreement with linear theory and a total electrostatic energy exponentiating as shown in Fig. 10(a). The spatially homogeneous component of the internal field, $E_{k=0}$, Fig. 10(b), remains very small out to $t = 2$, then increases rapidly and becomes approximately equal to the external field amplitude at $t = 4$. At this time, the spatially homogeneous component of the internal field effectively cancels the external field and the instability saturates. After saturation ($t > 4$), the electrostatic energy density condenses into solitons which remain stable for the duration of the computation ($t_{max} = 10$). Typical plots of the electrostatic energy density and of the ion density fluctuation are shown in Fig. 11 which corresponds to $t = 6$. Approximately 22 solitons may be counted on these plots with values of $k_0\lambda_D$ varying between 0.02 and 0.05. These solitons have an approximately uniform distribution in space and are stationary although the amplitudes of the individual solitons fluctuate.

The spectrum of the electric field is given in Fig. 12(a) at a particular instant, $t = 6$, and Fig. 12(b) shows the same spectrum averaged between $t = 6$ and $t = 9$ at intervals of 0.5. The solid line represents the spectrum of a single soliton, as in Fig. 9, with $k_0 = 4$, while the straight line represents the k^{-2} power law.

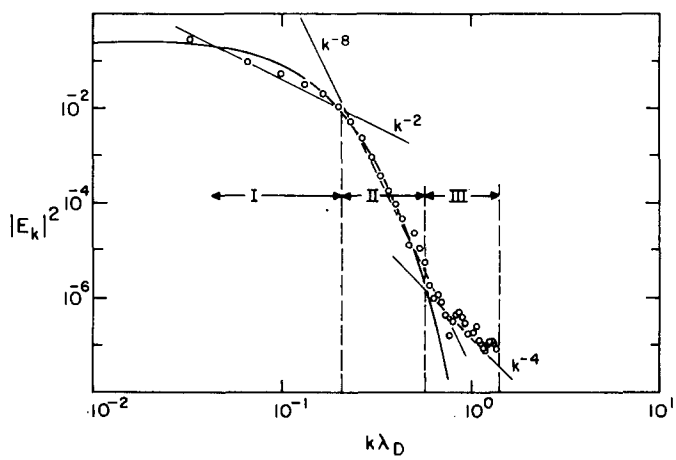

FIG. 9. Mode spectrum $|E_k|^2$ versus $k\lambda_D$. Circles correspond to the particle code driven by an external pump with $\eta = 0.16$ at $t = 18$. The solid curve is the spectrum of a soliton with $k_0 = 2$.

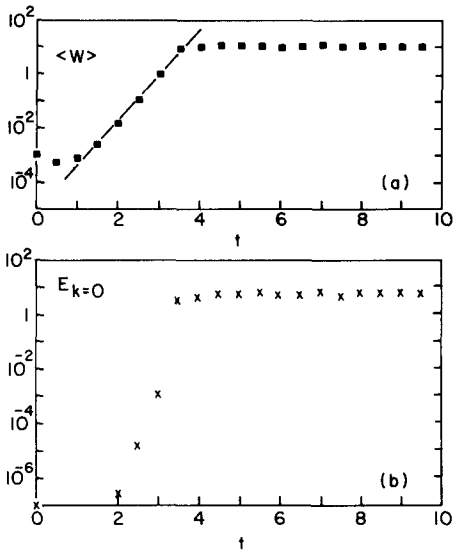

FIG. 10. (a) Total electrostatic energy as a function of time from the fluid code driven by an external pump field with normalized amplitude $\eta = 0.125$. The intermediate stage shows exponential growth of the parametric instability. (b) Spatially homogeneous component of the electric field versus time.

In this computation the solitons are long lived and clearly separated, with their number N remaining approximately constant in time. Thus, the spectrum should indeed be comparable to the spectrum of a single soliton, following an exponential, rather than a power law, as a function of k.

For stronger pump fields, larger and narrower solitons are generated initially but do not remain stable. Solitons generated with a pump field $\eta = 0.25$ are shown in Fig. 13, which corresponds to a small region of space $80 \leq x \leq 85.4$. After saturation, distinct solitons are observed at $t = 2$, see Fig. 13(a). These large-amplitude solitons break up for $t > 2$, after which new soliton-like structures having smaller amplitudes, reappear as shown in Fig. 13(b). This is typical of later

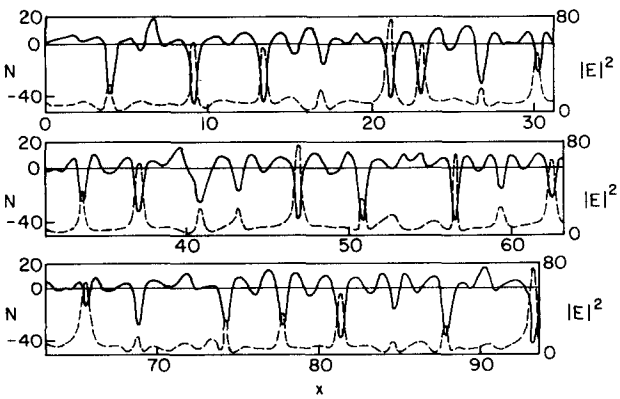

FIG. 11. Electrostatic field energy (broken line) and ion density fluctuation (solid line) at $t = 6$ for the fluid code driven by an external pump with $\eta = 0.125$. The scale at left is for the ion density, at right for the electrostatic energy density. The length of the system is 97.6 in dimensionless coordinates. Approximately 22 solitons, and a background of ion waves are observed.

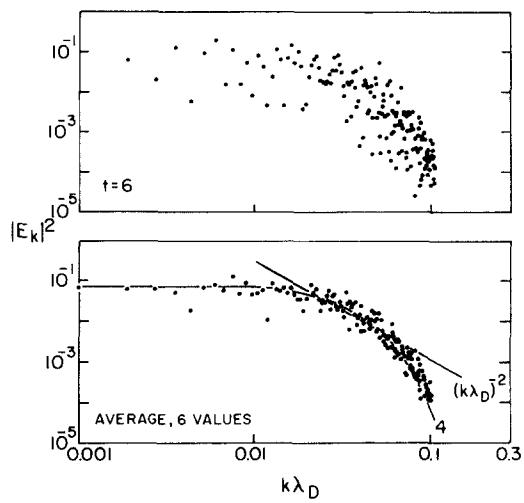

FIG. 12. (a) Mode spectrum $|E_k|^2$ versus $k\lambda_D$ for $\eta = 0.125$ at $t = 6$. (b) Average mode spectrum versus $k\lambda_D$. The solid line is the spectrum of a soliton with dimensionless parameter $k_0 = 4.0$, suitably normalized.

times in the computation, where individual soliton-like structures disappear and are continuously regenerated. Note that in this later stage, the correlation between ion density depletion and energy density is not as clear as in the early stage. This behavior is in agreement with the recently published results of Morales and Lee.[27]

The theory of Kingsep *et al.*[9] is based on two hypotheses, viz., (i) that the electric field after saturation of the instability would condense into a system of solitons, and (ii) that the system would pass through all possible

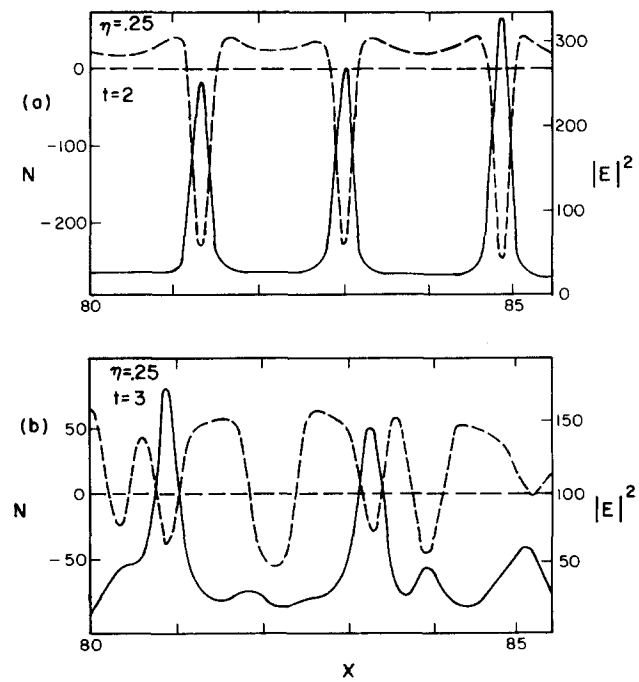

FIG. 13. Electrostatic field energy (broken line) and ion density fluctuation (solid line) at $t = 2$ and $t = 3$ for the fluid code driven by an external pump with $\eta = 0.25$. Only the region $80 < x < 85.4$ is shown.

states, with the number N of solitons ranging between a minimum N_{min} and a maximum N_{max}, with equal probability. The resulting soliton turbulence then yields an equilibrium spectrum which obeys a power law of the form k^{-2}.

For weak pump fields ($\eta \lesssim 0.25$), the fluid computations of this section show that, after saturation, the parametric instability indeed displays a system of solitons, and therefore verifies the first hypothesis of Kingsep *et al.* In this regime, however, the soliton structure is stable ($\eta = 0.125$, see Fig. 11), or at least number N of solitons remains constant in time ($\eta = 0.25$, see Fig. 13), and the second hypothesis is not verified. It follows that, in this case, the electric field spectrum $|E_k|^2$ fits a law of the form $\cosh^{-2} k$ as shown in Fig. 12. A particle simulation of the parametric instability in this regime ($\eta = 0.25$) by Denavit,[28] yields an electric field spectrum $|E_k|^2$ which falls as k^{-2} in the interval $0.07 \lesssim k\lambda_D \lesssim 0.2$, then falls as k^{-5} for $k\lambda_D \gtrsim 0.2$ [see Fig. 4(a) of Ref. 28]. However, it is clear that this overall spectrum would fit the law $\cosh^{-2} k$ better than any particular power law. This particle simulation is therefore in substantial agreement with the computations of this section, which were based on Zakharov's model, including Landau damping terms to account for resonant particle interactions.

For strong pump fields ($\eta \geq 0.5$), particle simulations have shown the existence of soliton-like structures,[26] and yield an electric field spectrum of the form $|E_k| \propto k^{-q}$ with $q \simeq 2$ out to $k\lambda_D \simeq 0.5$.[3,4,28] Therefore, the second hypothesis of the soliton turbulence theory appears to be satisfied only for sufficiently strong pump fields. In this regime, however, it is not clear that the introduction of simple damping terms, proportional to the Landau damping rates γ_k, properly represents resonant particle effects. For this reason, fluid computations for strong pump fields were not carried out and must await the formulation of a model which would account for nonlinear particle interactions.

Note added in proof: As this paper was going to press we were made aware of similar work by Y. S. Sigov and Y. V. Khodirev, Dokl. Akad. Nauk SSSR **229**, No. 4 (1976).

ACKNOWLEDGMENTS

This work was supported by the U. S. Energy Research and Development Administration under Contract E(11-1) 3170 to Cornell University and E(11-1) 2200 to Northwestern University.

[1]See for instance: B. B. Kadomtsev, *Plasma Turbulence* (Academic, New York, 1965); or R. C. Davidson, *Methods of Nonlinear Plasma Theory* (Academic, New York, 1972).
[2]S. Kainer, J. Dawson, and T. Coffey, Phys. Fluids **15**, 2419 (1972).
[3]J. J. Thomson, R. J. Faehl, and W. L. Kruer, Phys. Rev. Lett. **31**, 918 (1973); J. J. Thomson, R. J. Faehl, W. L. Kruer, and S. Bodner, Phys. Fluids **17**, 973 (1974).
[4]J. S. DeGroot and J. I. Katz, Phys. Fluids **16**, 401 (1973); J. I. Katz, J. S. DeGroot, and R. J. Faehl, *ibid.* **18**, 1173 (1975).
[5]L. E. Thode and R. N. Sudan, Phys. Rev. Lett. **30**, 732 (1973); Phys. Fluids **18**, 1552 (1975); **18**, 1564 (1975).
[6]A. A. Vedenov, A. V. Gordeev, and L. I. Rudakov, Plasma Phys. **9**, 719 (1967).
[7]V. N. Oraevskii and R. Z. Sagdeev, Zh. Tekh. Fiz. **32**, 1291 (1962) [Sov. Phys.-Tech. Phys. **7**, 955 (1963)].
[8]K. Nishikawa, J. Phys. Soc. Jpn. **24**, 916 (1968); J. Phys. Soc. Jpn. **24**, 1152 (1968).
[9]A. S. Kingsep, L. I. Rudakov, and R. N. Sudan, Phys. Rev. Lett. **31**, 1482 (1973).
[10]V. E. Zakharov, Zh. Eksp. Teor. Fiz. **62**, 1745 (1972) [Sov. Phys.-JETP **35**, 908 (1972)].
[11]J. Denavit, N. R. Pereira, and R. N. Sudan, Phys. Rev. Lett. **33**, 1435 (1974).
[12]G. Schmidt, Phys. Rev. Lett. **34**, 724 (1975); V. E. Zakharov and A. M. Rubenchik, Zh. Eksp. Teor. Fiz. **65**, 997 (1973) [Sov. Phys.-JETP **38**, 494 (1974)]; L. M. Degtyarev, V. E. Zakharov, and L. I. Rudakov, Zh. Eksp. Teor. Fiz. **68**, 115 (1975) [Sov. Phys.-JETP **41**, 57 (1976)].
[13]N. R. Pereira, Ph. D. thesis, Cornell University (1976).
[14]See for instance: L. D. Landau and E. M. Lifschitz, *Mechanics* (Pergamon, New York, 1960), Sec. 30; or M. E. Mahric, Phys. Fluids **18**, 837 (1975).
[15]L. I. Rudakov, Dokl. Akad. Nauk SSSR **207**, 821 (1972) [Sov. Phys. Dokl. **17**, 1166 (1973)].
[16]E. Ott and R. N. Sudan, Phys. Fluids **12**, 2388 (1969); **13**, 1432 (1970).
[17]A. G. Litvak, V. Yu. Traktengherts, T. N. Fedoseeva, and G. M. Fraiman, Zh. Eksp. Teor. Fiz. Pis'ma Red. **20**, 544 (1974) [JETP Lett. **20**, 248 (1974)].
[18]V. G. Makhankov, Phys. Lett. A **50**, 42 (1974).
[19]A. N. Kaufman, Phys. Scr. (Sweden) **11**, 303 (1975).
[20]J. Denavit, J. Comput. Phys. **9**, 75 (1972).
[21]Y. Matsuda and F. W. Crawford, Phys. Fluids **18**, 1336 (1975); **18**, 1346 (1975).
[22]R. H. Hardin and F. D. Tappert, SIAM Rev. **15**, 423 (1973); F. D. Tappert, in *Seventh Conference on Numerical Simulation of Plasmas* (Courant Institute, New York University, New York, 1975), p. 123.
[23]Kh. O. Abdulloev, I. L. Bogolubskii, and V. G. Makhankov, Phys. Lett. A **48**, 161 (1974).
[24]L. M. Degtyarev, V. G. Makhankov, and L. I. Rudakov, Zh. Eksp. Teor. Fiz. **67**, 533 (1974) [Sov. Phys.-JETP **40**, 264 (1975)].
[25]V. E. Zakharov and A. B. Shabat, Zh. Eksp. Teor. Fiz. **61**, 118 (1971) [Sov. Phys.-JETP **34**, 62 (1972)].
[26]E. J. Valeo and W. L. Kruer, Phys. Rev. Lett. **33**, 750 (1974).
[27]G. L. Morales and Y. C. Lee, Phys. Fluids **19**, 690 (1976).
[28]J. Denavit, Phys. Fluids **19**, 972 (1976).